

# Optimization of joining HDPE rods by continuous drive friction welding

Mohammed A. Tashkandi<sup>1,\*</sup>, Nidhal M. Becheikh<sup>2</sup>

<sup>1</sup>Department of Mechanical Engineering, Northern Border University, Arar, Saudi Arabia

<sup>2</sup>Department of Chemical and Materials Engineering, Northern Border University, Arar, Saudi Arabia

Continuous drive friction welding (CDFW) is a solid-state joining procedure that can be used to join various similar and dissimilar materials. High-density polyethylene (HDPE) is a thermoplastic that can replace many traditional materials. Utilizing experimental design procedures such as response surface method (RSM) is a reliable approach for determining the most significant process parameters and optimizing the desired responses. The current study employed an RSM experimental design to investigate the effects of the process parameters for welding HDPE rods using CDFW. The design evaluated the process parameters and three outcome responses: the maximum welding temperature, the axial shortening, and the tensile strength (TS). The combination of the three responses can allow achieving high-efficiency welds. The results showed that it was possible to achieve high-efficiency welds while maintaining axial shortening and controlling temperature. A TS >65% of the parent material's strength with an axial shortening of <3 mm was achieved.

Keywords: *continuous drive friction welding, RSM, HDPE, welding temperature, axial shortening, tensile strength*

## 1. Introduction

Continuous drive friction welding (CDFW) is a solid-state process that delivers many benefits, including environment friendliness, being more economical, and a significant reduction in the formation of intermetallic layers. Friction welding was first discovered in 1995 by Thomas *et al.* [1]. It branches into three main types: stir friction welding (SFW), stir spot friction welding (SSFW), and rotational friction welding (RFW). Two types of rotational friction welding emerged, inertia friction welding (IFW) and CDFW. The main difference between these two types of rotational friction welding is the application and duration of frictional forces or pressures.

CDFW is generally divided into two stages: a friction stage and a forging stage. The process begins with bringing the two parts to be welded into proximity. One side is attached to a flywheel to rotate at a specific rotational speed (RS) (rotating side). The other is attached to a pressure application apparatus and not allowed to turn (fixed

side). The friction stage is the portion of the process where the two surfaces to be welded together are rubbed against each other while one side continuously rotates. The other side is under a constant pre-determined force. The process is carried out for a specific time, depending on the welded material. After the completion of that time, the forging or upset stage is commenced by suddenly stopping the rotation and immediately applying a higher force for a pre-determined time that lasts until the end of the process.

Many studies have focused on CDFW of similar materials, specifically aluminum, and any process modifications that may affect the process. Abdulla *et al.* [2] studied the effects of time in the upset stage on the process of welding AA6061. The microstructure and mechanical properties of AA6060-T6 tubes were investigated in the study of D'Urso *et al.* [3]; the tensile strength (TS) and macrostructure were used to evaluate the effect of feed rate and the RS on the joint quality. Another study by Li *et al.* [4] analyzed the joint quality of AA6061-T6 rods through friction torque, temperature, microstructure, and axial shortening. The ef-

\* E-mail: tashkandi@gmail.com

fect of friction time on the joint quality based on TS and macrostructure for AA6061 was demonstrated in Tashkandi and Mohamed [5]. Yilbas *et al.*'s [6] study of friction-welded aluminum bars is among the first studies investigating friction welding for aluminum alloys.

Likewise, studies pertaining to the welding of dissimilar materials have been widely published, especially those that discuss welding steel alloys to aluminum alloys. In Sahin's study [7], austenitic stainless steel was welded to aluminum. Following the conclusion of the welding process, the welded joints were evaluated using statistical procedures, tensile tests, and microhardness tests. Reddy *et al.*'s study [8] is another example of a paper discussing dissimilar material welding, in this instance, welding of AA6061 and AISI 304. Hincapi *et al.*'s study [9] discusses the welding of aluminum and stainless steel, with a particular focus on controlling the formation of the Fe–Al interlayer; the welded joints obtained in this study are assessed by measuring welding temperature, evaluating TS, and microstructure evaluation.

The most recent research trends in CDFW studies investigated joint properties for metal matrix alloys. Hincapi *et al.* [9] and Adalarasan *et al.* [10] investigated CDFW of composite rods (Al/SiC/Al<sub>2</sub>O<sub>3</sub>). Various process parameters were incorporated in an experimental design (Taguchi L9 orthogonal), the objective being to assess the quality of the joints. The TS, as well as the elongation, was observed and used to optimize the joints. Another study by Celik and Gunes [11] considered joining AA365 and AISI 1030. The aluminum alloy was reinforced by SiC particulates. The quality of the joints was assessed based on TS, microhardness, and microstructural observations. Another study by Senthilkumar *et al.* [12] investigated the post-weld heat treatment effects on AA6061/SiC/graphite rods.

High-density polyethylene (HDPE) is a high-diffusion thermoplastic polymer. Polymer materials such as HDPE have many advantages that allow them to be attractive alternative materials, especially in corrosive environments or joint replacement parts. Friction welding of HDPE as either FSW or FSSW has been widely investigated. Gao

*et al.* [13] investigated the mechanical properties of joints made by FSW from HDPE-ABS as dissimilar materials. The effects of shoulder design in SFW of HDPE plates were analyzed [14]. The result of preheating on FSW of HDPE plates was investigated [15]. Also, the effects of the rotating speed, advancing speed, and pin design on butt-welded HDPE sheets was studied by Kaddour *et al.* [16]. Concerning the investigation of outcomes, most research papers focus on the welded joints' mechanical properties (tensile and microhardness). Additionally, they focus on the joints' macrostructure and microstructures and the thermodynamics involved while welding. There are also studies, e.g., Paoletti *et al.* [17], in which the forces and temperatures occurring in the FSW of polymers have been analyzed and reported.

A limited number of studies have investigated joining HDPE using CDFW. One study by Hasegawaa *et al.* [18] investigated joining polyethylene. It was stated that there were some similarities between joining carbon steel and polyethylene, like the theory that the total material loss increases with friction pressure. However, it was also stated that, unlike in the case of joining carbon steel, when it came to joining polyethylene, the upset length proportions on both sides of the welding depended on the prevalent welding conditions. Additionally, a narrow range of process parameter levels was mentioned where favorable-appearing joints could be achieved. The same authors published another study [19] where CDFW was implemented to join the branch and main gas pipes onsite without digging the paved road.

Statistical procedures such as experimental design can prove helpful in processes involving many levels and require design optimization. Some researchers implemented experimental designs to determine significant process parameters or levels or optimize the process. Most statistical experimental design studies consider using Taguchi analysis [10, 20–22]. Response surface method (RSM) offers a robust experimental design procedure. The statistical analysis allows for finding the most significant parameters and possible interactions. The resulting response surface plots also allow visualizing the relationship between process parameters

and measured responses. Experimental designs of CDFW of polymers have not been widely investigated in the literature. To the authors' knowledge, there are only a very few RSM investigations available concerning CDFW, and the ones concerning CDFW of HDPE number even fewer.

This paper explores the optimization of CDFW of HDPE using RSM, considering related process parameters and desirable process outcomes. The effect of the welding process parameters on joint quality is investigated. The joint quality assessment employing maximum welding temperature, axial shortening, and TS is reported.

## 2. Methodology

HDPE rods measuring 16 mm in diameter were procured from a local supplier. The properties of the HDPE used are listed in Table 1. The rods were cut into smaller segments (65 mm) to be used for the welding process. The surfaces to be welded were washed with distilled water and dried before the welding operation. CDFW of HDPE was conducted utilizing a lathe machine equipped with a pneumatic system fabricated in the laboratory to control the welding process parameters, as shown in Figure 1. The same setup was used for welding different materials, such as aluminum and steel, as indicated in Tashkandi and Mohamed [5]. Thus the present experimental setup that uses a lathe machine to perform the welding is valid.



Fig. 1. CDFW machine setup. CDFW, continuous drive friction welding

Table 1. Physical and mechanical properties of HDPE [23]

Property	Value
Melting temperature (°C)	126–135
Crystallization temperature (°C)	111.9
Density (g/cm <sup>3</sup> )	0.955
Thermal conductivity (W/mK)	0.35–0.49
Specific heat – solid (kJ/kg°C)	1.9
Tensile strength (MPa) at 23°C	23.0–29.5

The main parameters that can influence the friction welding procedure are the time of friction, the friction force, the rotating speed, the upset force, and the upset time. Since the literature on CDFW of HDPE is limited, and the ranges of the welding parameters can be very large, a series of trial runs were conducted. The purpose was to narrow the parameter ranges according to the requirements of welding such material. Preliminary results indicated that very high rotating speeds (>1,000 rpm) and very high friction force led to failed joints. Very high RS's or excessive friction force cause wear in the material instead of softening it at temperatures below its melting temperature, thus preventing welding.

The trial-and-error experiments also indicated that the RS's and friction force should be <600 rpm and 2,000 N, respectively. The runs did not reveal any noticeable effects in the joint's quality or appearance caused by the upset force and the upset time. Hence, upset time and force were not considered process parameters investigated in this study and were kept constants for all the study runs.

### 2.1. Response surface methodology

The process parameters chosen for this work were the time of friction ( $t_f$ ), friction force ( $F_f$ ), and RS. The time and pressure factors were evaluated as continuous factors. In contrast, the RS was assessed as a categorical factor due to the limited speed options provided in the lathe machine. Preliminary welding experiments indicated that very high RS's lead to poor joints [17], while material ejection caused by very high rotating speeds leads to poor welded joints. Thus, RS values were chosen as the settings on the lathe machine under 600 rpm.

The experimental design is given in Table 2. The welding parameters were abbreviated as indicated by the column "Code."

Table 2. Levels of process parameters for CDFW of HDPE

Parameter	Code	Levels
RS (rpm)	Speed	82 – 169 – 300 – 400 – 550
Friction force – $F_f$ (N)	Force	1,000–2,000
Friction time – $t_f$ (s)	Time	30–60

The experimental design was a two-level full design, with a total number of runs of 65, consisting of 20 cubic points, 25 center points within the cube, and 20 axial points. It was run in a single block and with a single replication with an alpha level of 1.14. The order of the runs was randomized, and experiments were run according to the randomized order.

The responses used to evaluate the process parameters were the maximum welding temperature recorded during the experiment, the axial shortening, and the joint's TS. The welding flash and axial shortening formation are directly related to the heat generated and the maximum welding temperature. Combining the heat generated, the axial shortening, and TS may be an appropriate technique to identify the range of parameters that influence the welds' quality and provide an insight into optimal process parameters.

The temperature was measured using an IR Dual Laser Point Thermometer at the contacting surfaces. It had an operational range of  $-50^{\circ}\text{C}$  to  $800^{\circ}\text{C}$ , a spatial accuracy of 1 mm, and a time accuracy of 0.5 s. The device can be calibrated according to the emissivity of the measured material. The emissivity was adjusted accordingly, and the thermometer was calibrated successfully before any temperature measurement. The maximum contact temperature was recorded and tabulated for each run. The axial shortening was determined by measuring the length of the samples before and after the welding procedure. All length measurements were performed using a Vernier caliper. Tensile testing was accomplished using a universal tensile testing machine according to ASTM D638-14 [24].

Figure 2 shows the dimensions of the tensile test specimen. All tensile tests were carried out at a 5 mm/min rate. The ultimate TS reading for each sample was used in the RSM analysis. All statistics were performed using Minitab® 19 with a confidence level of 95%.

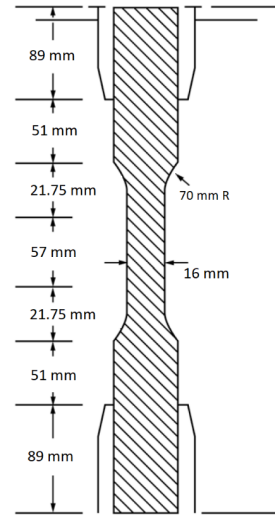


Fig. 2. Tensile test specimen dimensions

### 3. Results

All welding runs were completed within one session to minimize any variation that could arise if the samples were welded in patches. The welding order was followed according to the randomized order outcome from the statistical software. Figure 3 shows welded samples at various process conditions resulting in different flash formations.

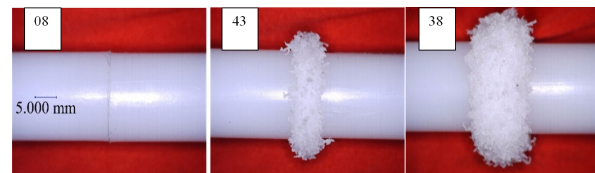


Fig. 3. HDPE rods joined using CDFW according to different welding conditions. CDFW, continuous drive friction welding; HDPE, high-density polyethylene

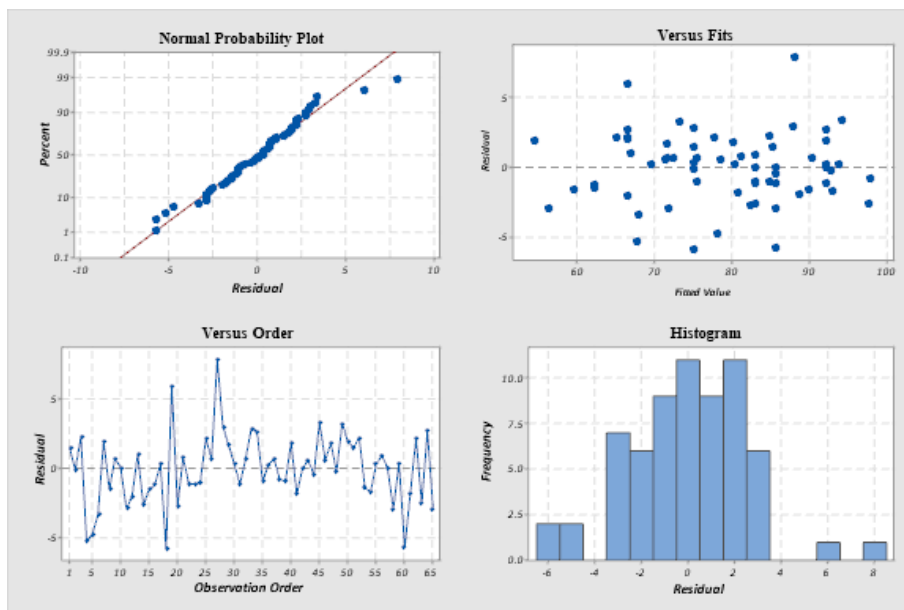


Fig. 4. Data normality check using the normal probability plot, the versus fits, the histogram, and the versus order for  $T_{max}$

Table 3. Analysis of variance

Source	DF	Adj SS	Adj MS	F-Value	P-Value
Model	17	7297.99	429.29	50.12	0.000
Linear	6	7162.50	1193.75	139.37	0.000
$t_f$	1	1510.42	1510.42	176.34	0.000
$F_f$	1	467.61	467.61	54.59	0.000
RS	4	5184.47	1296.12	151.32	0.000
Square	2	92.92	46.46	5.42	0.008
$T_f^2$	1	40.66	40.66	4.75	0.034
$F_f^2$	1	63.98	63.98	7.47	0.009
2-Way Interaction	9	42.58	4.73	0.55	0.828
$t_f * F_f$	1	18.43	18.43	2.15	0.149
$t_f * RS$	4	20.98	5.24	0.61	0.656
$F_f * RS$	4	3.17	0.79	0.09	0.984
Error	47	402.56	8.57		
Lack-of-Fit	27	287.51	10.65	1.85	0.080
Pure Error	20	115.06	5.75		
Total	64	7700.56			

Table 4. Regression equation in coded parameters

RS	Regression equation
082	$T_{max} = 9.91 + 1.003t_f + 0.02847F_f - 0.00481t_f^2 - 0.000006F_f^2 - 0.000130t_f \times F_f$
165	$T_{max} = 16.14 + 0.998t_f + 0.03025F_f - 0.00481t_f^2 - 0.000006F_f^2 - 0.000130t_f \times F_f$
300	$T_{max} = 21.83 + 1.070t_f + 0.02963F_f - 0.00481t_f^2 - 0.000006F_f^2 - 0.000130t_f \times F_f$
400	$T_{max} = 22.80 + 1.111t_f + 0.02948F_f - 0.00481t_f^2 - 0.000006F_f^2 - 0.000130t_f \times F_f$
550	$T_{max} = 35.17 + 0.988t_f + 0.02932F_f - 0.00481t_f^2 - 0.000006F_f^2 - 0.000130t_f \times F_f$

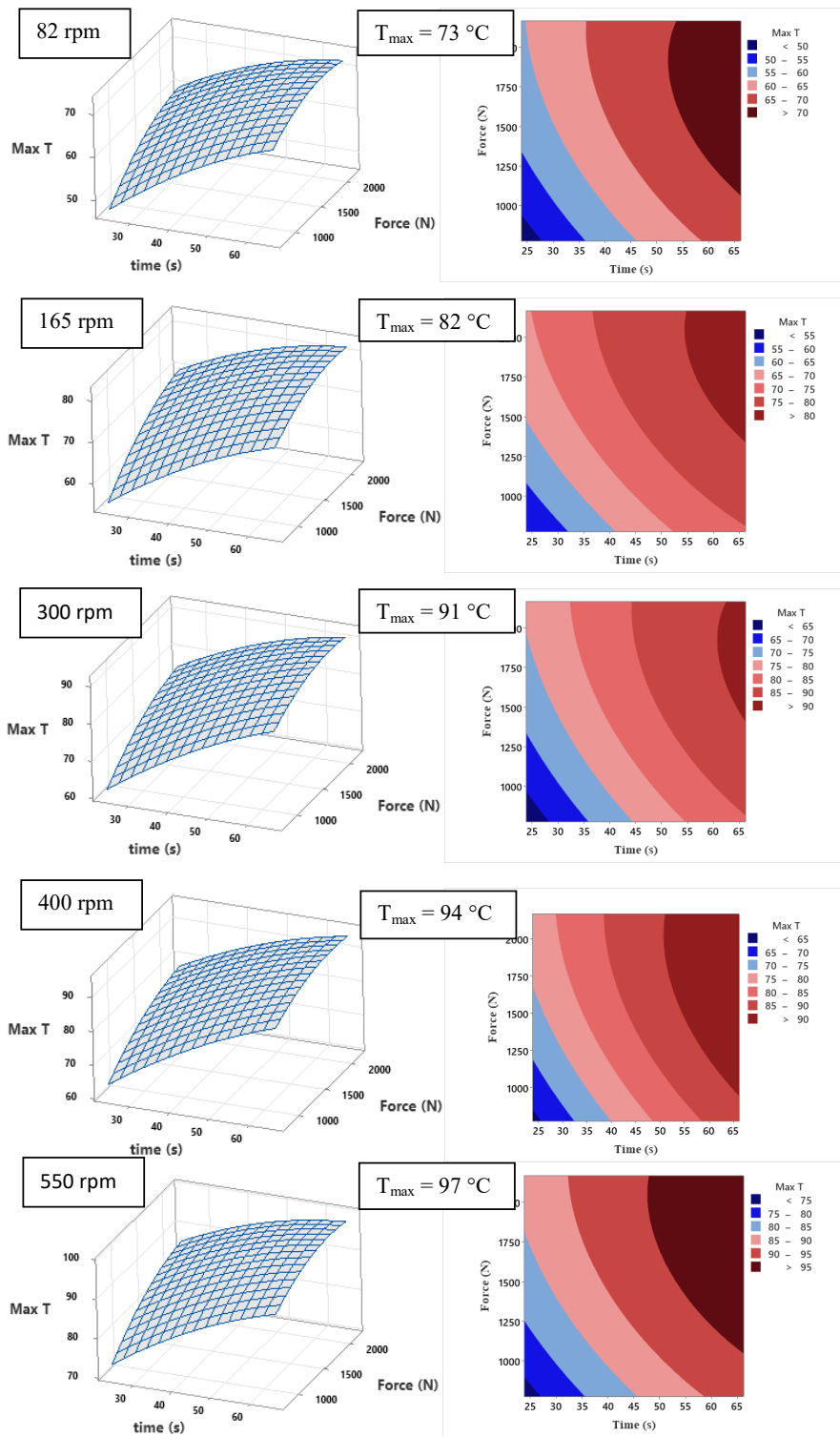


Fig. 5. 3D surface and contour plots for the maximum welding temperature. The maximum reported values are actual measured values for each speed level

### 3.1. RSM of the maximum welding temperature

$T_{max}$  data were measured, recorded, and then used to evaluate the RSM design. Figure 4 relates to testing the normality of the data. Data analysis demonstrates the validity of the assumption that the data are normal and validates the choice of statistical procedures needed. Table 3 shows the analysis of variance (ANOVA) results for the  $T_{max}$ . The fitted model is statistically significant ( $P$ -value = 0). ANOVA also indicates that all welding process parameters are statistically significant, with the  $t_f$  and RS having more weight since their  $F$ -value is greater than  $F_f$ . The two-way interactions are statistically insignificant. Moreover, the lack of fit test is statistically insignificant, indicating that the fitted model is appropriate.

Table 4 shows the regression equations for each of the five RS's. It can be noted that the value of the constant-coefficient increases as the RS increases. The linear terms' coefficients are much more significant than the square terms' coefficients or the two-way interactions between the factors. The surface and contour plots are used for visualizing and understanding the process parameters' effects. Figure 5 shows the surface and contour plots of the welding process parameters according to the RS.

It can be seen that  $T_{max}$  increases as the RS increases. Moreover, the contour plots show the ranges of  $F_f$  and  $t_f$  where different ranges of  $T_{max}$  can be achieved. All surface and contour plots of all RS's indicated that maximum temperatures are achieved for a high level of  $F_f$  and  $t_f$ . The model estimates a maximum temperature of about 73°C for an RS of 82 rpm and 82°C at 165 rpm. At 300 rpm and 400 rpm, the attainable  $T_{max}$  values were about 91°C and 94°C, respectively. Finally, at 550 rpm,  $T_{max}$  is expected to be as high as about 97°C.

As RS increases from 82 rpm to 550 rpm, the noticeable differences in the  $T_{max}$  value are invariably accompanied by corresponding changes in the contours. The welding temperature can never be >80°C and 90°C for 82 rpm and 165 rpm, respectively. On the contrary, the temperature can reach up to 100°C for the three remaining levels of RS.

Likewise, there is a "cold region" for the 82-rpm case where the temperature does not exceed 50°C, at very low values of  $F_f$  and  $t_f$ . The lowest temperature range observed in each case increases in value as RS increases. As seen in the contour plots for 550 rpm, the lowest temperature range is 70–80°C located within the region confined to the contour corresponding to 1,250 N and 35 s. If producing the highest welding temperature were to be considered an objective. The inference can be made from the contour plots that using the CDFW technique by setting the RS to 300 rpm, 400 rpm, or 550 rpm would enable joints to be welded at temperatures very close to 100°C. The 550 rpm contour plots indicate broad ranges of  $F_f$  and  $t_f$  for reaching such high welding temperatures.

### 3.2. RSM of the axial shortening

The axial shortening was analyzed in the statistical design as a second response. Figure 6 shows the plots of the design used to check for data normality. It is evident that the assumption of the data being normal is valid; hence, the validity of the statistical analysis and regression model is satisfied. Most of the data are located on a straight line in the normal probability plot. There is no evident order of the data in the versus fits and versus order plots. Finally, the histogram plots' data distribution resembles a "bell-shaped" curve that supports the data's normality assumption.

Table 5 shows the results of the ANOVA for the axial shortening. The statistical analysis in Table 5 shows that friction time is the most statistically significant parameter affecting the axial shortening of CDFW of HDPE rods. The  $t_f$  registered a very high  $F$ -value of 586.87 and a  $p$ -value <0.05. The RS was the second most statistically significant parameter since it had a large  $F$ -value of 475.77 and a  $p$ -value <0.05. The friction force was statistically significant with a  $p$ -value <0.05 but had much less effect than the other process parameters.

The square terms in the ANOVA table representing the continuous parameters' square levels indicate that  $t_f^2$  is statistically insignificant since the  $p$ -value is >0.05, and that  $F_f^2$  is statistically significant. The two-way interaction among the process

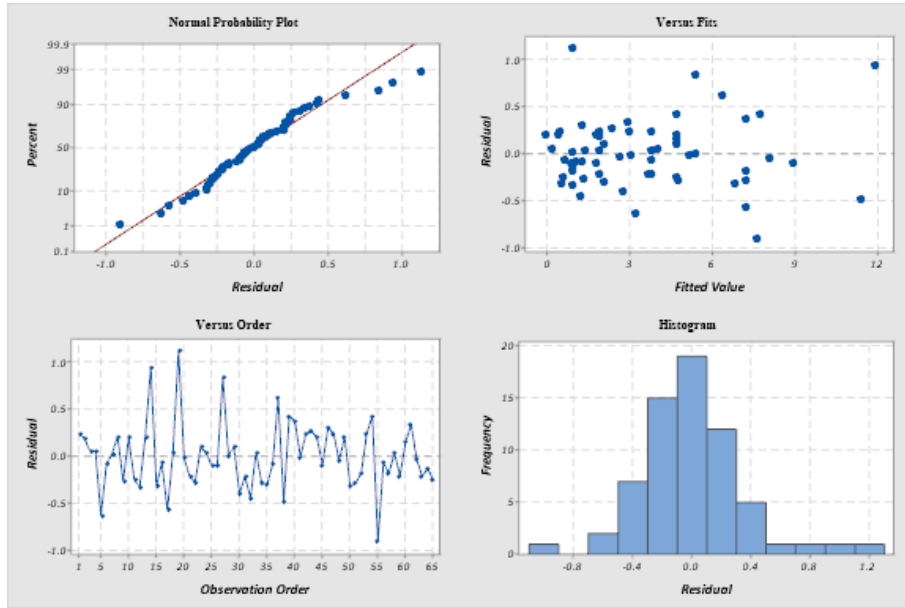


Fig. 6. Data normality check using the normal probability plot, the versus fits, the histogram, and the versus order for the axial shortening

Table 5. Analysis of variance for the axial shortening

Source	DF	Adj SS	Adj MS	F-Value	P-Value
Model	17	492.737	28.9845	174.17	0.000
Linear	6	445.319	74.2199	446.00	0.000
$t_f$	1	97.663	97.6626	586.87	0.000
$F_f$	1	30.961	30.9606	186.05	0.000
RS	4	316.696	79.1740	475.77	0.000
Square	2	1.404	0.7021	4.22	0.021
$t_f^2$	1	0.006	0.0058	0.03	0.853
$F_f^2$	1	1.352	1.3516	8.12	0.006
2-Way Interaction	9	46.014	5.1126	30.72	0.000
$t_f * F_f$	1	3.486	3.4861	20.95	0.000
$t_f * RS$	4	37.344	9.3360	56.10	0.000
$F_f * RS$	4	5.184	1.2959	7.79	0.000
Error	47	7.821	0.1664		
Lack-of-Fit	27	5.567	0.2062	1.83	0.084
Pure Error	20	2.254	0.1127		
Total	64	500.559			

Table 6. Regression equation in coded parameters for the axial shortening

RS (rpm)	Regression equation
082	Short = $1.06 - 0.0717t_f + 0.00064F_f + 0.000057t_f^2 - 0.000001F_f^2 + 0.000057t_f \times F_f$
165	Short = $-0.60 - 0.0400t_f + 0.00147F_f + 0.000057t_f^2 - 0.000001F_f^2 + 0.000057t_f \times F_f$
300	Short = $-2.43 + 0.0312t_f + 0.00183F_f + 0.000057t_f^2 - 0.000001F_f^2 + 0.000057t_f \times F_f$
400	Short = $-1.75 + 0.0494t_f + 0.00141F_f + 0.000057t_f^2 - 0.000001F_f^2 + 0.000057t_f \times F_f$
550	Short = $-4.07 + 0.1086t_f + 0.00290F_f + 0.000057t_f^2 - 0.000001F_f^2 + 0.000057t_f \times F_f$

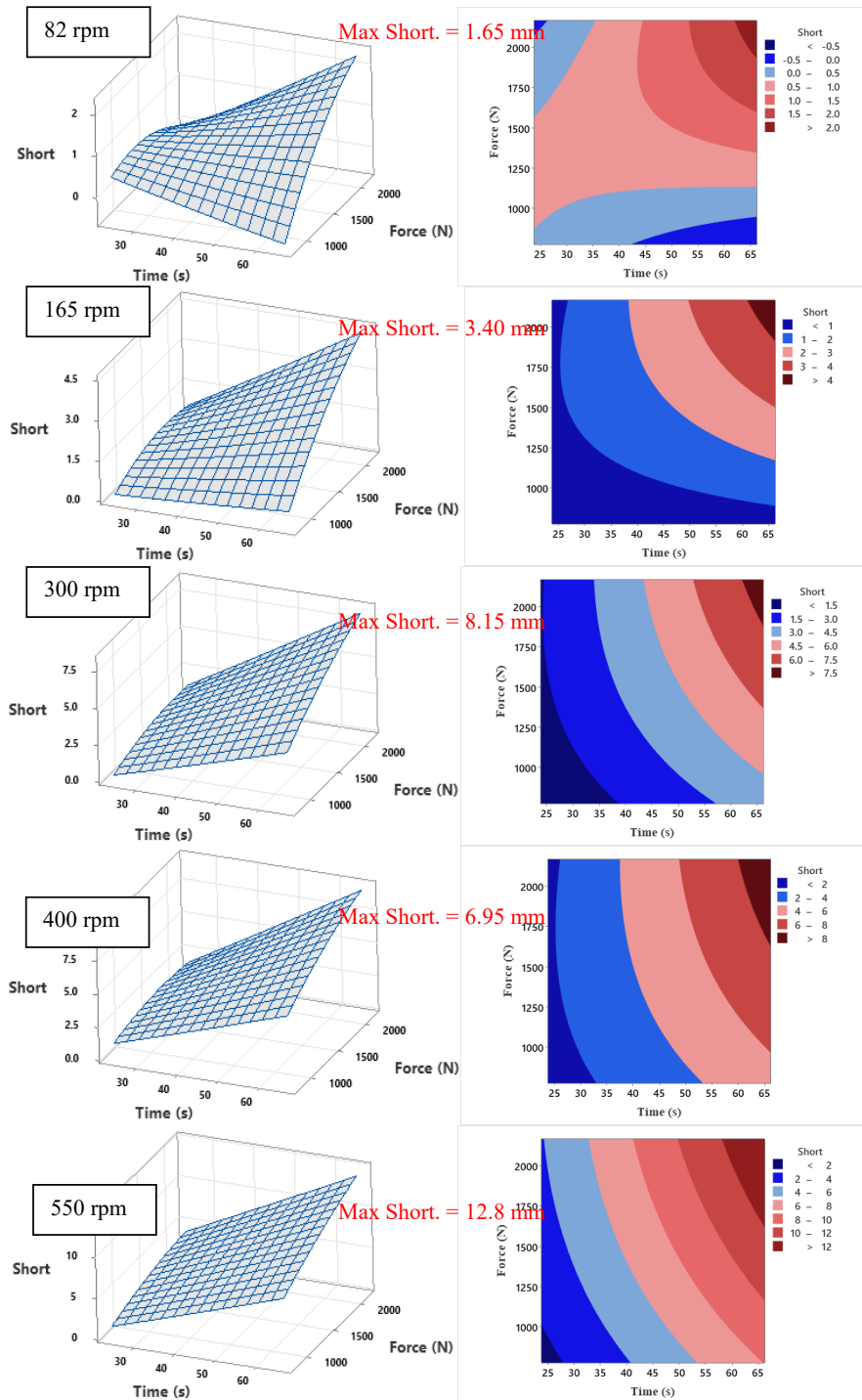


Fig. 7. 3D surface and contour plots for the axial shortening according to RS's. The maximum reported values are actual measured values for each speed level

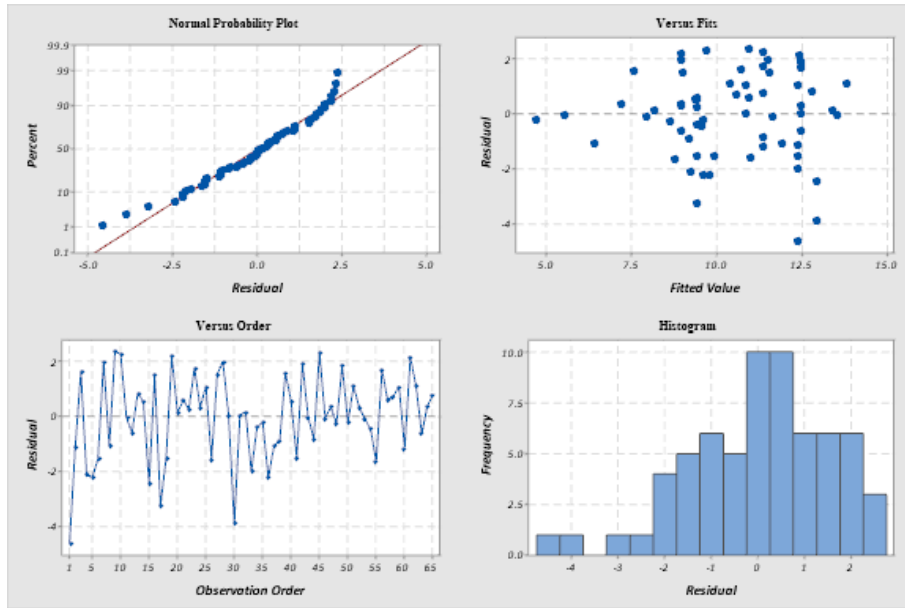


Fig. 8. Data normality check using the normal probability plot, the versus fits, the histogram, and the versus order for the TS. TS, tensile strength

Table 7. ANOVA for TS

Source	DF	Adj SS	Adj MS	F-Value	P-Value
Model	17	243.893	14.347	4.34	0.000
Linear	6	163.399	27.233	8.25	0.000
$t_f$	1	4.031	4.031	1.22	0.275
$F_f$	1	17.543	17.543	5.31	0.026
RS	4	141.825	35.456	10.74	0.000
Square	2	8.616	4.308	1.30	0.281
$T_f^2$	1	4.475	4.475	1.36	0.250
$F_f^2$	1	5.260	5.260	1.59	0.213
2-Way Interaction	9	71.878	7.986	2.42	0.024
$t_f * F_f$	1	2.833	2.833	0.86	0.359
$t_f * RS$	4	42.229	10.557	3.20	0.021
$F_f * RS$	4	26.816	6.704	2.03	0.105
Error	47	155.205	3.302		
Lack-of-Fit	27	108.605	4.022	1.73	0.106
Pure Error	20	46.600	2.330		
Total	64	399.098			

Table 8. Regression equations for predicting the TS

RS (rpm)	Regression equation
082	$TS = -10.61 + 0.345t_f + 0.00959F_f - 0.00159t_f^2 - 0.000002F_f^2 - 0.000051t_f \times F_f$
165	$TS = 3.10 + 0.256t_f + 0.00532F_f - 0.00159t_f^2 - 0.000002F_f^2 - 0.000051t_f \times F_f$
300	$TS = -2.41 + 0.224t_f + 0.01012F_f - 0.00159t_f^2 - 0.000002F_f^2 - 0.000051t_f \times F_f$
400	$TS = 3.13 + 0.131t_f + 0.00842F_f - 0.00159t_f^2 - 0.000002F_f^2 - 0.000051t_f \times F_f$
550	$TS = -4.04 + 0.242t_f + 0.00859F_f - 0.00159t_f^2 - 0.000002F_f^2 - 0.000051t_f \times F_f$

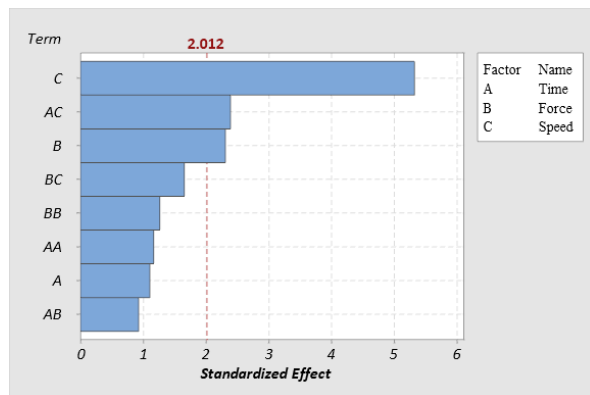


Fig. 9. Pareto chart of the standardized effects for the TS of the joints. TS, tensile strength

parameters results in the ANOVA table indicated that all interactions are statistically significant ( $p$ -value  $< 0.05$ ). The interaction between  $t_f$  and RS appears to be the parameter interaction with the maximum impact since its  $F$ -value is much higher than the other interactions. Table 6 shows the regression equations for estimating the axial shortening corresponding to rotational speed. It can be observed that the coefficients of all square variables and the two-way interaction are the same regardless of the rotational speed being considered. Also, a rotational speed of 82 rpm had the lowest  $F_f$  coefficient, whereas 550 rpm had the highest  $F_f$  coefficient. On the other hand, 300 rpm had the lowest  $t_f$  coefficient, and 550 rpm had the highest  $t_f$  coefficient.

Figure 7 shows the surface and contour plots for the axial shortening for all levels of RS. At 82 rpm, there seems to be a “saddle” region in the surface plots, and the axial shortening never exceeds 2 mm. Minimum axial shortening occurs at very large or very small values of  $t_f$  combined with very small or very large values of  $F_f$ . However, the stated observation may not be significant since the maximum axial shortening is not expected to exceed 2 mm. The surface and contour plots indicate that the upper limit of axial shortening seems to increase gradually. However, minimal axial shortening values are still observed even for very high RS's. At 165 rpm, the maximum axial shortening is about 4.5 mm at very high values of  $t_f$

and  $F_f$ . The exact process parameters settings (very high  $t_f$  and  $F_f$ ) produced maximum axial shortening for the remaining RS levels; about 7.5 mm at 300 rpm, about 7.8 mm at 400 rpm, and about 14 mm at 550 rpm. The results strongly suggest that axial shortening increases with increasing all three process parameters, but still, narrow regions exist where minimal axial shortening can be achieved. Furthermore, there is no significant difference in the axial shortening among RS levels of 300 rpm and 400 rpm since surfaces and contour plots for these two speeds are very similar.

### 3.3. RSM of the TS

The joints' TS was evaluated as the third and final response in the experimental design. As mentioned in the methodology section, the TS data collected were tabulated and analyzed. Figure 8 shows the validity of the assumptions required for the RSM analysis. All plots within the figure indicate that the assumption of normal data distribution is satisfied, thus demonstrating the validity of the analysis. The factors' effects and corresponding levels on the Pareto chart are illustrated in Figure 9. Since the chart displays the effects' absolute value, one cannot predict the factors' effects. Instead, it indicates the relatively large effects caused by the factors. The figure suggests that the RS has the most considerable effect on TS. The interaction between friction and RS has the second-largest effect, and the frictional force has the third-largest effect.

The ANOVA results of the analysis are indicated in Table 7. The results show the significance of the model that predicts the TS ( $p$ -value of 0.000). The linear terms and the two-way interactions are statistically significant in this model, with  $p$ -values of 0.000 and 0.024, respectively. The most statistically significant process parameter is RS ( $F$ -value of 10.74 and a  $p$ -value of 0.000), followed by the  $F_f$  ( $F$ -value of 5.31 and  $p$ -value of 0.026), and finally, the two-way interaction of  $t_f$  and RS ( $F$ -value of 3.2 and  $p$ -value of 0.021). The “lack of fit” term indicated no lack of fit in the results since the  $p$ -value for this term was 0.106.

The model also predicts the TS's expected val-

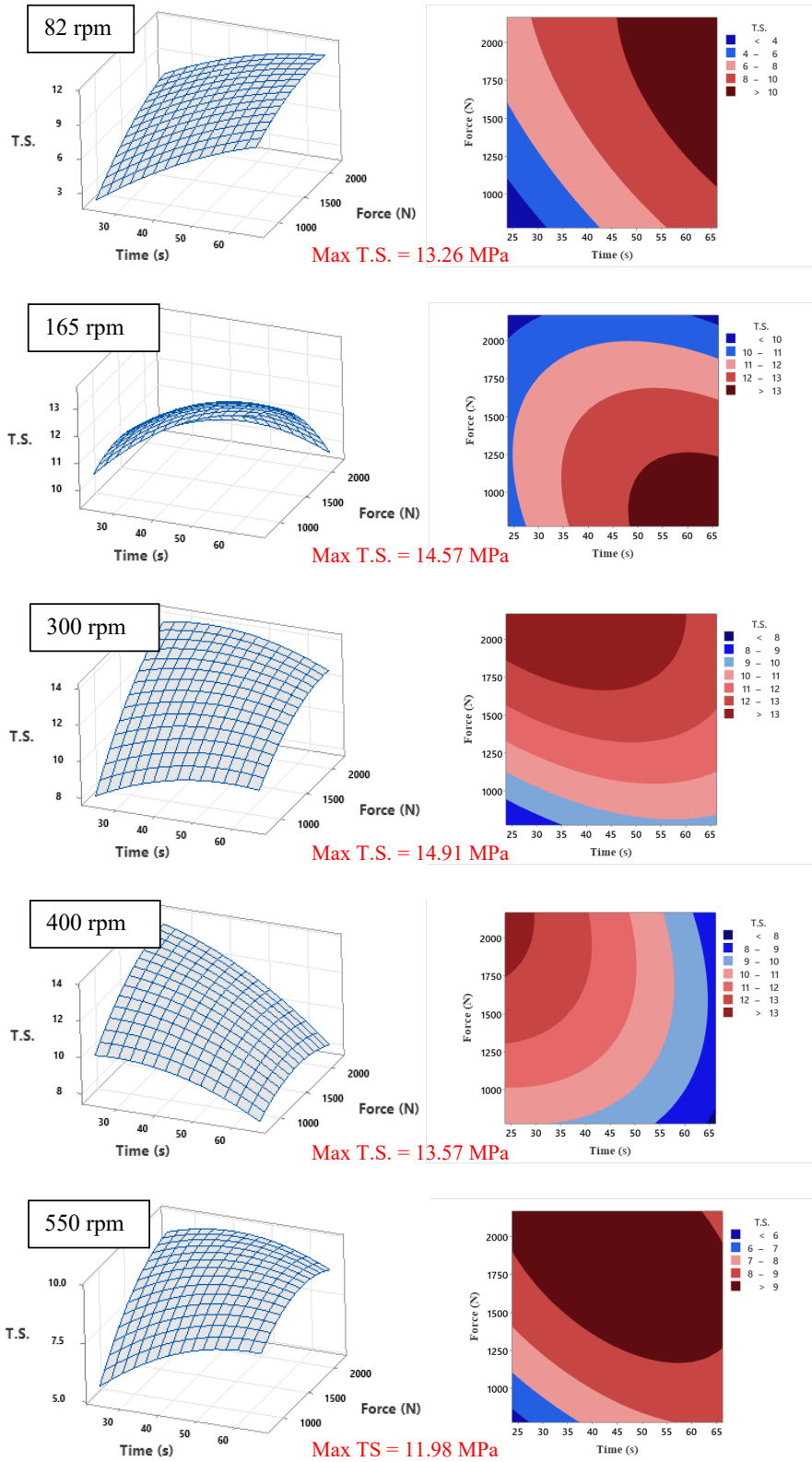


Fig. 10. Surface and contour plots of the TS as a function of  $t_f$  and  $F_f$ . The maximum reported values are actual measured values for each speed level

ues for all process parameters, as indicated in Table 8. The constant-coefficient suggests that the TS is expected to be very low at 82 rpm, followed by 550 rpm and 300 rpm. On the other hand, the RS's of 165 rpm and 400 rpm seem to allow the TS to reach its maximum potential value. The coefficients of the square and two-way interaction terms agree with the ANOVA results, suggesting that these terms' effects on predicting the TS are not as prominent as the linear terms.

Figure 10 shows the surface and contour plots for the TS as a function of all process parameters being studied. At 82 rpm, the maximum predicted TS is about 12 MPa, which can be achieved by choosing  $t_f$  and  $F_f$  levels corresponding to the contour plot's upper right corner (high force and high time). As the speed increases to 165 rpm, the maximum achievable predicted TS is 14 MPa in the lower right corner of the contour plot (low force and high time). The 300 rpm plots indicate that a TS of 14 MPa can also be achieved for a wide range of  $t_f$  (25 s to ~60 s) when the  $F_f$  is about 2,000 N or higher. The same TS value can be achieved at 400 rpm but for a much narrower time window (25 s to ~28 s) with the same high force value. Finally, the maximum achievable TS for 550 rpm decreases to about 10 MPa or less, as shown in the figure.

## 4. Discussion

The maximum welding temperature depends mainly on the friction time and the RS since these two parameters had the highest  $F$ -values. The friction force's contribution to  $T_{max}$  is less than the other parameters. Hence, increasing or decreasing  $T_{max}$  can be achieved mainly by adjusting  $t_f$  and RS.

The heat generation at any moment during the CDFW process is governed by Eq. (1) as given by Can *et al.* [25], where  $r$  is the radius of the material,  $P$  is the friction pressure (force divided by area), and  $\omega$  is the RS. Under similar process conditions and materials, the rotating speed contributes to the heat generation more than the frictional force, which is also observed in the regression equations in Table 4. All constant coefficients

are positive and increase with increasing RS. Increasing the temperature beyond the maximum observed value seems possible by increasing the rotating speed and the friction time without changing the force. Such an increase may increase the plasticity of the material and lead to better welding quality.

$$\dot{q} \left( \frac{W}{m^2} \right) = \pi r P \omega \quad (1)$$

The RSM analysis for the axial shortening indicated that all process parameters significantly affect the response outcome. In addition, the interaction between RS and  $t_f$  was the most significant two-way interaction (highest  $F$ -value). The expected axial shortening is minimal at very low speeds and reaches a maximum value of about 2 mm with very high  $F_f$  and  $t_f$ . The saddle-like feature indicates that most of the shortening observed for this speed is expected to be between 0.25 mm and 1 mm. As the speed increases, the saddle vanishes, and axial shortening increases linearly as the other process parameters increase. The outlined result is logical since axial shortening is directly related to the material being consumed within the contact interface during the process. According to the results, the best way to have minimum axial shortening is to use very low RS's regardless of the other process parameters.

A different situation was observed to prevail in the case of the tensile strength response. For  $T_{max}$  and the axial shortening, all surface and contour plots followed a similar pattern as the speed increased from 82 rpm to 550 rpm. The only difference was with regard to the fact that the maximum recorded response was observed to increase each time. As for TS, the peak location changes with speed and does not have a linear relationship with speed, i.e., it does not increase with increasing RS. The TS of the joints made by CDFW for HDPE depends significantly on all process conditions, and there seems to be a space of process parameter levels where maximum TS can be achieved. Any decreasing or increasing process parameters outside that space reduce the TS significantly. The regression equations' coefficients, the surface, and contour plots suggested that maximum TS can be

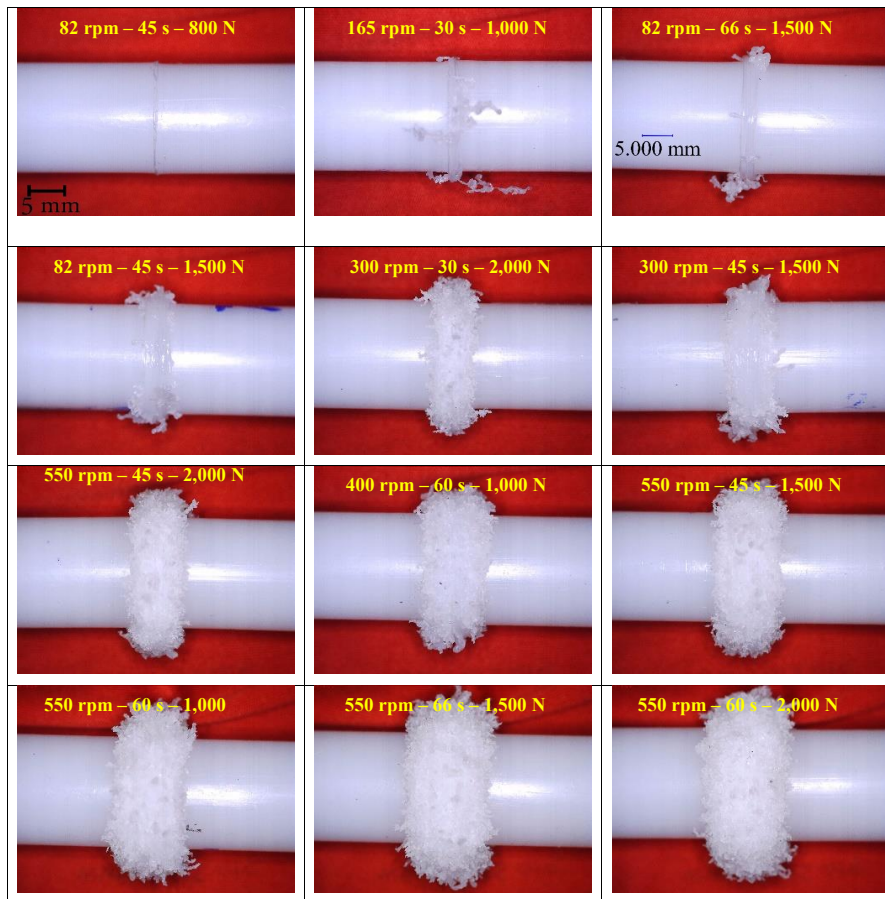


Fig. 11. Effect of process parameters on the appearance of welded joints arranged according to axial shortening from minimum to maximum

achieved with either 300 rpm or 400 rpm, with a more extensive range of process parameter levels for 300 rpm, as indicated in Figure 8.

The maximum TS achieved was 14.9 MPa, about 66% of the TS of unwelded HDPE. The maximum TS is relatively close to that in other studies [13–16, 19]. The joints of HDPE made by CDFW seem to have the best TS for an RS level of 300 rpm. The median value of RS being the most suitable indicates a balance in the material consumption within this speed and the heat generated that led to the highest joint efficiency. Being a rotational process that depends on radial distance, the rods' central parts requiring welding are the most difficult to weld [26].

Moreover, the maximum TS was achieved by either very high speed and low friction time or

very low speed and very high friction time. This indicates that the material within these settings becomes suitable for forming strong bonds and, thus, strong joints. As it happens, the axial shortening is affected in the same way the least axial shortening was observed in these conditions. Usually, the outer regions are welded, and the central part remains unwelded. At 300 rpm with various levels of process parameters, the results are inductive that a considerable portion of the contact surfaces is welded. Figure 11 compares the shapes of the welded joints corresponding to various process conditions. The images were arranged from top left to bottom right according to axial shortening from 0.15 mm to 12.8 mm at approximately 1 mm intervals.

## 5. Conclusion

The current study investigated joining rods made of HDPE material using CDFW. Experimental design through RSM analysis was used to statistically explore the ranges of process parameters and responses of interest. Through 65 experiments, the evaluation and prediction of the effects of the process parameters on  $T_{max}$ , axial shortening, and TS were accomplished. The following observations are concluded:

- The RS and friction time affect the maximum welding temperature and axial shortening more than the friction force.
- The TS depends on the RS and friction force since the friction time was statistically insignificant.
- An RS of 300 rpm was the most appropriate rotating speed for achieving the desired outcomes.
- TS of >65% of the material's TS was acquired for a vast range of process parameters.
- The welding temperature was high enough to form a good joint without reaching the material's melting point.
- Minimum axial shortening was also achieved, which is a desirable outcome since material losses would be minimal while maintaining strength.

Future work can achieve higher percentages of joint TS without compromising axial shortening and considering the interface's maximum welding temperature.

### Conflicts of interest

Not applicable.

### Availability of data and materials

Statistical data are included in Appendix A.

### Authors' contributions

M.T. performed the literature review, experimental design, data collection, and analysis and drafted the manuscript. N.B. performed experiments, collected and analyzed the data, and drafted the manuscript.

## Acknowledgements

The authors acknowledge the funding received for this research from the Deanship of Scientific Research at Northern Border University under grant No. ENG-2018-3-9-F-7808.

## References

- [1] Thomas WM, Nicholas ED, Needham JC, Murch MG, Temple-Smith P, Dawes CJ. Friction welding. 1995.
- [2] Abdulla F, Irawan Y, Darmadi D, Azzawiya Oil Refining Company, Brawijaya U. Tensile strength and Macro-microstructures of A6061 CDFW weld joint influenced by pressure and holding time in the upset stage. *J ReKayasa Mesin*. 2018; 9:149–54; <https://doi.org/10.21776/ub.jrm.2018.009.02.12>.
- [3] D'Urso G, Longo M, Giardini C. Microstructure and mechanical properties of Friction Stir Welded AA6060-T6 tubes. *Current State-Of-The-Art on Material Forming: Numerical and Experimental Approaches at Different Length-Scales, Pts 1-3*. 2013;554–557:977–84; <https://doi.org/10.4028/www.scientific.net/KEM.554-557.977>.
- [4] Li X, Li J, Jin F, Xiong J, Zhang F. Effect of rotational speed on friction behavior of rotary friction welding of AA6061-T6 aluminum alloy. *Weld World*. 2018; 62:923–30; <https://doi.org/10.1007/s40194-018-0601-y>.
- [5] Tashkandi MA, Mohamed ML. Effect of friction time on the mechanical and microstructural properties of AA6061 joints by continuous drive friction welding. *Eng Technol Appl Sci Res*. 2020; 10:5596–602; <https://doi.org/10.48084/etasr.3438>.
- [6] Yilbas BS, Sahin AZ, Coban A, Abdul Aleem BJ. Investigation into the properties of friction-welded aluminium bars. *J Mater Process Technol*. 1995; 54:76–81; [https://doi.org/10.1016/0924-0136\(95\)01923-5](https://doi.org/10.1016/0924-0136(95)01923-5).
- [7] Sahin M. Joining of stainless-steel and aluminium materials by friction welding. *Int J Adv Manuf Technol*. 2009; 41:487–97; <https://doi.org/10.1007/s00170-008-1492-7>.
- [8] Reddy MG, Rao SA, Mohandas T. Role of electro-plated interlayer in continuous drive friction welding of AA6061 to AISI 304 dissimilar metals. *Sci Technol Weld Joining*. 2008; 13:619–28; <https://doi.org/10.1179/174329308x319217>.
- [9] Hincapi OD, Salazar JA, Restrepo JJ, Torres EA, Graciano-Urbe JA. Weldability of aluminum-steel joints using continuous drive friction welding process, without the presence of intermetallic compounds. *Eng J*. 2020; 24:129–44; <https://doi.org/10.4186/ej.2020.24.1.129>.
- [10] Adalarasan R, Santhanakumar M, Sundaram AS. Investigation in solid-state joining of Al/SiC/Al<sub>2</sub>O<sub>3</sub> composite using Grey-based desirability (GBD) and response surface plots. *J Chin Inst Eng*. 2017; 40:55–65; <https://doi.org/10.1080/02533839.2016.1271287>.
- [11] Celik S, Gunes D. Continuous drive friction welding of Al/SiC composite and AISI 1030. *Welding J*. 2012;

- 91:222S–8S.
- [12] Senthilkumar J, Suresh Mohan Kumar P, Balasubramanian V. Post weld heat treatment of continuous drive friction welded AA6061/SiC/graphite hybrid composites-an investigation. 2019. *Mater. Res. Express.*; 6(12), 1265e1; <https://doi.org/10.1088/2053-1591/ab6407>.
- [13] Gao J, Li C, Shilpakar U, Shen Y. Improvements of mechanical properties in dissimilar joints of HDPE and ABS via carbon nanotubes during friction stir welding process. *Mater Des.* 2015; 86:289–96; <https://doi.org/10.1016/j.matdes.2015.07.095>.
- [14] Mustapha K, Abdessamad B, Azzeddine B, Mokhtar Z. Experimental investigation of friction stir welding process on high-density polyethylene. *J Fail Anal Preven.* 2020; 20:590–6; <https://doi.org/10.1007/s11668-020-00867-0>.
- [15] Rehman RU, Sheikh-Ahmad J, Devenci S. Effect of preheating on joint quality in the friction stir welding of bimodal high density polyethylene. *Int J Adv Manuf Technol.* 2021; 117:1–14; <https://doi.org/10.1007/s00170-021-07740-w>.
- [16] Kaddour H, Hadj Miloud M, El Bahri OC, Abdallah L. Mechanical behavior analysis of a friction stir welding (FSW) for welded joint applied to polymer materials: mechanical behavior analysis of a friction stir welding (FSW) for welded joint applied to polymer materials. *Frattura ed Integrita Strutturale.* 2019; 13:459–67; <https://doi.org/10.3221/IGF-ESIS.47.36>.
- [17] Paoletti A, Lambiase F, Di Ilio A. Analysis of forces and temperatures in friction spot stir welding of thermoplastic polymers: analysis of forces and temperatures in friction spot stir welding of thermoplastic polymers. *Int J Adv Manuf Technol.* 2016; 83:1395–407; <https://doi.org/10.1007/s00170-015-7669-y>.
- [18] Hasegawaa M, Asadab T, Ozawa Y. Study of friction welding of polyethylene. *Welding Int.* 2002; 16:537–43.
- [19] Hasegawaa M, Yamaguchib Y, Uminob A, Furukawaa Y, Asadab T, Ozawa Y. Development of joining method of polyethylene branch pipe for gas and non-excavation construction method. *Welding Int.* 2015; 29:279–84.
- [20] Kalsi NS, Sharma VS. A statistical analysis of rotary friction welding of steel with varying carbon in workpieces. *Int J Adv Manuf Technol.* 2011; 57:957–67; <https://doi.org/10.1007/s00170-011-3361-z>.
- [21] Ramalingam A, Muthuvel S. Identification of optimal condition for solid state welding of Al/SiCp composite using Taguchi principles integrated TOPSIS (TPIT) method. *Int J Manuf Mater Mech Eng.* 2017; 7:19–37; <https://doi.org/10.4018/IJMMME.2017040102>.
- [22] Singh KJ. Multi-objective optimization of high carbon steel (EN-31) and low carbon steel (SAE-1020) using Grey Taguchi method in rotary friction stir welding. *Grey Syst Theory Appl.* 2019; 9:385.
- [23] Thakare KA, Vishwakarma HG, Bhawe A. Experimental investigation of possible use of HDPE as thermal storage material in thermal storage type solar cookers. *Int J Res Eng Technol.* 2015; 4:92–9.
- [24] ASTM D638-14. Standard test method for tensile properties of plastics. 10th ed. West Conshohocken, PA, USA: ASTM International; 2014.
- [25] Can A, Sahin M, Kucuk M. Modeling of friction welding. International Scientific Conference (UNITEC 10), Gabrovo, 19–20 November 2010.
- [26] Maalekian, M. Friction welding critical assessment of literature. *Sci Technol Welding Joining.* 2007; 12:738–59; <https://doi.org/10.1179/174329307x249333>.

**APPENDIX A: DATA**

Run	Maximum temperature (°C)	Axial shortening (mm)	Tensile strength (MPa)	Run	Maximum temperature (°C)	Axial shortening (mm)	Tensile strength (MPa)
1	56.3	0.15	4.450	34	86.8	4.45	14.910
2	62.4	0.20	7.102	35	81.9	3.55	12.514
3	60.8	0.65	7.800	36	82.0	3.80	12.790
4	72.3	1.65	9.390	37	83.0	4.00	14.370
5	53.3	0.30	5.510	38	84.0	3.70	14.150
6	73.0	1.00	13.260	39	80.5	3.55	11.830
7	58.0	0.15	5.320	40	73.2	2.15	10.870
8	64.5	0.95	8.356	41	95.9	6.20	10.500
9	69.1	0.75	9.320	42	80.6	2.35	9.040
10	64.4	0.55	8.330	43	91.3	8.15	9.090
11	68.6	0.70	9.250	44	76.4	1.95	14.300
12	72.4	2.00	11.110	45	94.1	6.70	7.100
13	68.4	0.90	10.930	46	73.3	2.55	7.390
14	61.0	0.50	13.030	47	90.8	5.35	13.470
15	76.0	0.75	13.550	48	85.2	4.85	10.500
16	68.8	1.35	11.290	49	79.9	4.80	10.160
17	81.8	3.40	11.520	50	85.7	4.85	13.570
18	67.1	0.75	11.910	51	82.7	4.40	12.110
19	79.0	3.25	14.570	52	84.5	4.75	13.060
20	67.9	0.55	13.620	53	81.8	3.20	7.490
21	79.9	2.55	11.450	54	92.6	8.00	8.330
22	74.9	2.05	11.240	55	86.8	5.10	7.900
23	75.4	1.65	13.410	56	95.0	12.80	9.890
24	69.2	1.90	10.820	57	79.6	3.00	8.290
25	77.9	1.90	10.340	58	97.0	10.90	8.270
26	76.5	2.10	7.730	59	83.8	5.10	9.120
27	69.7	1.15	7.540	60	97.6	8.80	11.980
28	87.0	4.05	12.285	61	94.9	6.90	8.980
29	79.0	2.60	13.500	62	92.5	6.60	6.140
30	88.3	6.45	10.500	63	92.2	7.00	9.970
31	72.0	1.55	11.560	64	94.1	7.55	9.930
32	91.0	6.95	10.810	65	91.1	6.90	9.650
33	74.4	1.70	9.360				

*Received 2022-01-13**Accepted 2022-05-30*